**Article:**
Wilson, LA, Heraty, L, Ashford, BA et al. (5 more authors) (2021) Tissue microarray (TMA) use in post mortem neuropathology. Journal of Neuroscience Methods, 347. 108963. ISSN 0165-0270

https://doi.org/10.1016/j.jneumeth.2020.108963

**Tissue Microarray (TMA) Use in Post Mortem Neuropathology.**

*Research Paper*

Wilson LA[1], Heraty L[2], Ashford BA[3], Coelho S[4, 5], Frangi AF[5, 6], Pozo JM[5], Ince PG[3] and Highley JR[3]

[1]Royal (Dick) School of Veterinary Studies, University of Edinburgh, Easter Bush Campus, Midlothian, EH25 9RG.

[2]UK Dementia Research Institute, Cardiff University, *Hadyn* Ellis Building, Maindy Road, Cardiff, CF24 4HQ.

[3]Sheffield Institute for Translational Neuroscience, University of Sheffield, 385A Glossop Road, Sheffield. S10 2HQ, UK.

[4]Center for Biomedical Imaging, Department of Radiology, New York University School of Medicine, NY, USA.

[5]Centre for Computational Imaging & Simulation Technologies in Biomedicine, School of Computing, University of Leeds, Woodhouse Lane, Leeds LS2 9JT, United Kingdom.

[6]Medical Imaging Research Center (MIRC), Department of Cardiovascular Sciences Department, KU Leuven, Campus Gasthuisberg, Herestraat 49, 3000 Leuven Belgium.

# 1 Abstract

**Background:**

Tissue microarrays (TMAs), where each block (and thus section) contains multiple tissue cores from multiple blocks potentially allow more efficient use of tissue, reagents and time in neuropathology.

**New Method:**

The relationship between data from TMA cores and whole sections was investigated using 'virtual' TMA cores. This involved quantitative assessments of microglial pathology in white matter lesions and motor neuron disease, alongside qualitative TDP-43 inclusion status in motor neuron disease cases. Following this, a protocol was developed for TMA construction.

**Results:**

For microglial pathology we found good concordance between virtual cores and whole sections for volume density using one 1.75mm core (equivalent to a 2mm core after accounting for peripheral tissue loss). More sophisticated microglial cell size and measures required two cores. Qualitative results of pTDP-43 pathology showed use of one 1.75mm core gave a 100% sensitivity and specificity within grey matter, and 88.3% sensitivity and 100% specificity within white matter. A method of producing the TMAs was suitable for immunohistochemistry both manually and by autostainer, with the minimal core loss from the microscope slide.

**Comparison with Existing Methods:**

TMAs have been used infrequently in post mortem neuropathology research. However, we believe TMAs give comparable tissue assessment results and can be constructed, sectioned and stained with relative ease.

**Conclusions:**

We found TMAs could be used to assess both quantitative (microglial pathology) and qualitative pathology (TDP-43 proteinopathy) with greatly reduced quantities of tissue, time and reagents. These could be used for further work to improve data acquisition efficiency.

## 2 Keywords

Tissue microarray; neuropathology; post mortem; neurodegeneration; formalin fixed paraffin embedded; immunohistochemistry.

## 3 Highlights

- Tissue microarrays can be used for quantitative and qualitative measures.
- Tissue microarray reliability assessment can be achieved virtually.
- Core loss was minimal (1.8%) using our methods.
- Tissue microarrays allow increased efficiency.

# 4 Introduction

Formalin fixed paraffin embedded (FFPE) tissues represent a key archival resource of well-characterised research material, which has been extensively used for a multitude of techniques. Over recent years, an increasing demand has developed to achieve ‘more with less’ (Goldstine et al., 2002). This lends itself well to the use of tissue microarrays (TMAs), due to the greater patient numbers that can be assessed simultaneously.

Modern TMAs are paraffin blocks that contain multiple cylindrical cores of FFPE tissue from multiple different sources. TMA production involves harvesting a number of cores from a region of interest (ROI) within a donor FFPE block. These are then incorporated into a blank paraffin ‘recipient’ block (Fowler et al., 2011; Kononen et al., 1998). After sectioning, these TMA blocks allow simultaneous analysis of all the cores on one slide (Hoos and Cordon-Cardo, 2001; Prins et al., 2014; Saggioro et al., 2014) (Error! Reference source not found.Error! Reference source not found.).

Early attempts to create TMAs arranged tissue cores in a ‘tissue straw’ or ‘sausage’, (Battifora, 1986); (Wen-Hui Wan et al., 1987). Further development resulted in cores embedded individually in a grid pattern (Kononen et al., 1998). Variations of this technique are used commonly within cancer research (Hoos and Cordon-Cardo, 2001); (Kononen et al., 1998); (Gillett et al., 2000). However, use within neuropathology research is considerably more limited and again, many studies pertain to neoplasia (Boulagnon-Rombi et al., 2017) (Saggioro et al., 2014). There have been fewer attempts to use TMAs in post mortem and neurodegenerative research, although some important work is beginning to establish this technology in this field (Martikainen et al., 2006; Wang et al., 2006), (Walker et al., 2017).

To accelerate TMA production, specific equipment is required to sample both the cores from the donor block and insert these into the recipient block. One such example of this is this is the “MTA 1” Manual Tissue Arrayer from Beecher Instruments (Fowler et al., 2011). However, earlier papers made successful use of custom made “stainless steel tubes”

(Kononen et al., 1998) or hypodermic needles (Gillett et al., 2000). The use of the commercial instruments ensures accuracy in depth and angle of core collection, allowing greater consistency whilst producing the TMA.

As with any technique, there are limitations that must be appreciated when interpreting results. One aspect is 'core loss' which relates to the tendency of sections to lose cores either from the TMA block or becoming detached from the microscope slide during sectioning or staining. This can vary greatly depending on the technique used, with some core losses as high as 10-12% (Walker et al., 2017) and some as low as 2.7-3.7% (Martikainen et al., 2006).

TMAs can be used to assess both quantitative and qualitative pathology: Quantitative measures may include the number of features such as cells or neuritic plaques, or area density, (the percentage area of the sampled tissue that stains positively). Qualitative measures include the presence or absence of a given feature such as a particular pathological inclusion or lesion.

As only small sample cores are assessed by a TMA, it must be ensured that these are representative of the larger full section. Smaller diameter cores are susceptible to under representation of a given histological feature in heterogeneous tissues (Gillett et al., 2000; Hoos and Cordon-Cardo, 2001; Wang et al., 2006). For heterogeneous features, it may be suitable to use larger-diameter cores, or multiple cores from a donor block to allow a more accurate representation of the larger region. This issue can be assessed by undertaking some form of concordance (reliability) measurement

The aim of this project was to investigate and establish methods for using TMAs to assess neuropathology in post mortem tissue: We firstly wished to assess the degree to which the smaller quantity of tissue which can be assessed via a TMA core reflects the 'gold standard' of a full, conventional tissue section. This concordance assessment was addressed using whole slide images of digitised conventional microscope slides. The whole section was first

assessed, followed by one or more “virtual cores” corresponding to the areas sampled by the TMA needles. The measures from these virtual cores were then compared to measures from the whole section.

For this, two forms of pathology were investigated: 1) microglial changes in age-related white matter lesions and motor neurone disease (quantitative measures) 2) TDP-43-positive inclusions in motor neurone disease (qualitative measures). *Whilst a diverse range of immunohistochemical markers are utilised within neuropathology research, it is beyond the scope of this paper to analyse these in their entirety. Microglial markers and TDP-43 were chosen as these represent diverse features of pathology which are frequently assessed in neuropathological practice, and relevant to ongoing research interests within our group. The use of both age-related white matter and motor neuron disease lesions allowed two assessments of quantitative pathology, whilst use of TDP-43 enabled qualitative assessment.*

We then proceeded to develop a protocol for the construction, cutting and staining of post mortem brain TMAs.

Microglia are the predominant immune cells within the central nervous system (CNS) (Lasiene and Yamanaka, 2011). In their physiological state, microglia have a ramified morphology, whereas upon activation they proliferate, adopt an amoeboid morphology and change the molecular markers they express (Boche et al., 2013). Microglia are implicated in the pathogenesis and propagation of a number of neurodegenerative diseases (Malaspina et al., 2015; Saberi et al., 2015; Simpson et al., 2007). While the precise mechanisms vary between and within diseases, it is clear that they may be both inflammatory and toxic or anti-inflammatory and neuroprotective (Malaspina et al., 2015)(Tang and Le, 2016). *The alteration of microglial immunophenotype to an activated state can be demonstrated by immunohistochemistry. Increases in CD68 immunolabelling are observed in phagocytic microglia whilst MHCII immunolabelling is increased in pro-inflammatory microglia (Ashford*

*et al., 2020) and resting, homeostatic, pathogen sampling microglia can be identified with Iba-1 (Ashford et al., 2020).*

White Matter (WM) lesions are commonly seen on Magnetic Resonance Imaging of the elderly and are associated with cognitive impairment and depression in the ageing brain (Prins and Scheltens, 2015; Tully et al., 2017). The prevalence of these lesions increases with age (De Leeuw et al., 2001). DSCL (Deep Subcortical Lesions) show greater CD68 immunolabelling (a marker of phagocytic microglia) and alteration to an amoeboid morphology with a concomitant reduction in myelin (Simpson et al., 2007). Patients with DSCLs often have further microglial changes in other locations where there is no abnormality visible with MRI. These regions are often termed normal appearing white matter (NAWM) (Waller et al., 2019). The cause of the lesions remains unclear, with pathogenic pathways suggested involving hypoxia and blood brain barrier dysfunction amongst others (Fernando et al., 2006; Hainsworth et al., 2017).

Motor Neuron Disease (MND) was first identified in the 1850s (Veltema, 1975) presenting as a progressive paralysis leading to respiratory compromise and death within 2-3 years (Renton et al., 2014). 10% of cases are familial, with varying age of onset and progression depending, in part, on the mutation (Renton et al., 2014).

The major pathological hallmark of disease pathology is the presence of *aggregates of* ubiquitin-positive, *cytoplasmic inclusions comprising primarily of* 43kDa TAR DNA-binding protein (TDP-43). These inclusions are present in neurons and oligodendroglia (Arai et al., 2006; Ince et al., 2011; Neumann et al., 2006). *TDP-43 inclusions have also been demonstrated in a number of other neuropathological processes (Kovacs, 2019), which enables data gathered here to be relevant for a wide range of neuropathological studies.*

The aim of this project was to investigate and establish the use of TMAs to assess pathology in post-mortem human neurodegenerative disease. Firstly, we assessed the feasibility of a quantitative measure of microglial pathology in two disease processes (white matter lesions

in the ageing brain and motor neuron disease). Secondly, we assessed the qualitative attribute of the presence vs absence of TDP-43 inclusion pathology in tissues from motor neurone disease cases. This required ascertaining the concordance of the TMA with the full section for each measure. Alongside this, an effective and reliable method of TMA production was developed.

# 5 Methods

## 5.1 White Matter Lesion Microglial Quantitative Assessment

Before using a TMAs, it must be established that data from the smaller cores within the TMA are representative of data from the corresponding full section. We assessed this by using previously-immunolabelled and digitised sections of white matter lesions, analysed using an application established for this purpose in the Visiopharm image analysis platform (Visiopharm (Hoersholm-Denmark, 2017)). Details of the images used for this analysis can be seen in Coelho et al., 2018 and Waller et al., 2019. The slides had been immunolabelled for the microglial markers Iba-1, CD68 and MHCII. The algorithm on which the application for assessing shape is based can be seen in Waller et al., 2019. In brief, digitised whole microscope slide images were available from white matter from three groups: Control (non-lesional white matter from a brain in which no white matter lesions were present); deep subcortical lesions (DSCL); normal-appearing white matter (NAWM; white matter that did not appear to be lesional on MRI or to the naked eye but from a brain where DSCL where present elsewhere).

The following calculations were included within the application and recorded separately for each ROI.

1. Area density as a percentage coverage of the microglial labels as a proportion of the whole ROI. This was assessed for all three microglial immunohistochemistry labels, Iba-1, CD68 and MHCII.

$$Area\ Density = \left(\frac{Total\ Area\ of\ Microglial\ Labels}{Total\ Area\ of\ All\ Labels}\right) \times 100,$$

2. Average CD68-positive microglial profile size was calculated having excluded any profile of area less than 26.45µm$^2$. This reference value was selected to reduce bias due to data from incomplete microglial profiles (e.g. small processes that form part of a cell).

$$Average\ Microglial\ size = \left(\frac{Total\ Area\ of\ Microglial\ Labels\ (excluding\ those{<}26.45\mu m^2)}{Number\ of\ Microglial\ Labels\ (excluding\ those{<}26.45\mu m^2)}\right),$$

3. A shape metric was calculated for CD68-positive cells with larger values representative of larger sized and more rounded microglia and lower values representing smaller, more ramified microglia. For each labelled microglial profile of size >26.45µm$^2$, this was calculated by:

$$Microglial\ Shape\ Metric = Ci\ \frac{Ai-Ao}{Ao}\ where\ Ci = \frac{4\pi Ai}{p^2},$$

Ci is the profile's roundness (proximity to true circle), Ai is the profile's area, Ao is the cut-off value (26.45µm$^2$) and P is the profile's perimeter length.

This application was used to assess five cases from each of the control, DSCL (deep subcortical lesion) and NAWM (normal appearing white matter surrounding these lesions) groups. This tissue came from the deep white matter of the hemisphere (largely centrum semiovale). *Blocks were sampled from three coronal slices of approximately 1cm thickness from the level of: the head of the caudate nucleus (anterior slice); the lateral geniculate nucleus (middle slice) and tip of occipital horn of the lateral ventricle (posterior slice). This results in each block containing a number of Brodmann areas within deep grey matter, equidistant from the targeted white matter region. For further details, see supplementary figure 3.*

Digitised whole slide images from one Iba-1, one CD68 and one MHCII immunolabelled FFPE (formalin fixed paraffin embedded) section were analysed from each case. These included regions representing the total white matter within that section (the whole ROI). In

the control and NAWM sections this ROI consisted of the entirety of the white matter, apart from that immediately underlying to the cortex or at the periphery of the section (allowing 1-2mm clearance). For the DSCL sections this ROI incorporated the extent of microglial activation and alteration to an amoeboid phenotype as in Hainsworth et al., 2017.

Within the ROI, three circular 'virtual cores' of 1.75mm diameter were assessed. 1.75mm was used to mimic a section from a tissue which was taken with a 2mm diameter punch, but where the very periphery of the section was unanalysed to eliminate 'edge' artefact (Error! Reference source not found.). *Whilst larger cores have been used previously in neuropathology TMAs, such as 3mm (Walker et al., 2017), 2mm cores were selected as these are the largest available commercially for the Beecher MTA-1 Tissue Microarrayer which was used for the following physical TMA construction (See section 5.5). Furthermore, this method attempted to minimise tissue consumption, therefore minimising core size whilst maintaining accuracy was paramount.*

The mean of three, two or one virtual core(s) was calculated. A digital random number generator was used to select which virtual cores were included for two or one virtual core groups.

Correlations between measurements from the whole ROI and varying virtual core sizes and numbers were assessed. Kolmogorov-Smirnov goodness of fit test (KS) revealed many of the data sets deviated from the normal distribution. Thus, non-parametric statistical analyses were used. Correlations were assessed by Spearman's rank correlation co-efficient (*two-tailed*).

While correlation assesses the tendency for increases and decreases in two metrics to be related to each other, any consistent over or underestimation (bias) *and appreciation of the data ranges are difficult to appreciate* with this method. Thus agreement between virtual core data and the gold standard whole ROI was investigated by Bland-Altman plots (BAs) (Altman and Bland, 1983). *These allow comparisons between the 'gold standard' measure of the*

*whole ROI (x-axis) and the measures gained from one, two or three 2mm virtual cores (y-axis).* As many of the datasets were not normally distributed (by KS test), *analysis was* based on defining acceptable 'error ranges' for differences between the gold standard/whole ROI and the virtual core measures (Bland and Altman, 1999; Gagliardi et al., 1992; O'Brien et al., 1993).

These '10% error' and '5% error' ranges were calculated from the range of the whole ROI measurements (the x-axis of the Bland-Altman plots), and then calculating a difference of +/- 5% or 10% to establish the '5% error' and '10% error'. If obvious outliers were present in the whole ROI data, these were not included to allow a greater stringency in the error range.

These Bland-Altman plots were used to count the number of virtual TMA core measures that lay outside the 5% and 10% error ranges, thereby assessing the 'accuracy' of the virtual TMA core measurements. This is expressed in terms of the proportion of data points that lie within either 5% or 10% error ranges ('limits'): These measures were termed the '±5% accuracy' and '±10% accuracy' respectively, and were expressed as percentages of virtual core data points within the limits.

These accuracies were interpreted in light of intergroup differences between the means of the ROIs. Thus, if the difference in a given measure between two groups is small, a greater accuracy would be required for a study than if there are larger intergroup differences.

## 5.2 Spinal Cord Quantitative Assessment of Microglia in MND.

This assessment was performed on archived CD68 immunolabelled spinal cord sections. Separate ROIs of the lateral corticospinal tracts, the anterior horn, and the dorsal columns corresponded to the whole ROI 'gold standard' measurement (***Figure 2***). These areas were assessed using the same Visiopharm application as in the WM analysis, and an average of the left and right ROIs gave the measurements for the whole ROI.

This was performed on 11 post-mortem cases at varying anatomical levels of spinal cord from sporadic MND patients of varying disease onset and severity. Numerous slides

contained multiple sections from the same case, which were analysed separately giving a total of 20 sections.

Analysis of concordance proceeded in the same manner as the WM lesion analysis.

## 5.3 Cortical Quantitative Assessment of Microglia in MND

Due to the common finding of microglial pathology within the cortex of MND cases (Brooks et al., 2000), an assessment was performed using cortical sections. This was again undertaken virtually using digitised CD68 immunolabelled cortical sections and 1.75mm virtual cores, with measurements of microglial area density, profile size and shape metric as previously. This included analysis of seven MND motor cortex sections, three MND frontal cortex sections and three cortical sections of white matter lesion cases to provide a large amount of variability. Concordance assessment continued using BAs as described above, with three 1.75mm cores positioned randomly within the whole cortical ROI (***Figure 2***).

## 5.4 MND Quantitative pTDP-43 Assessment

Neuropathology often requires qualitative assessments, such as the presence or absence of a given feature. These features can be quite heterogeneous in their dispersion, posing a particular challenge for TMAs. TDP-43 pathology can be seen in a number of neurodegenerative conditions, but most importantly, MND and frontotemporal lobar degeneration. We wished to investigate whether TMAs could be used to assess TDP-43 pathology. This was investigated by assessing sections of grey and white matter from various forebrain regions that had been immunolabelled for phosphorylated TDP-43 (pTDP-43; 2B Scientific/Cosmo Bio, antigen retrieval by pressure cooker at pH6; 1h incubation of primary antibody at room temperature and dilution of 1:4000; A.Menarini Intellipath kit).

We assessed a series of samples with variable burdens of pTDP-43 pathology. Sections were from various forebrain areas from cases of MND, frontotemporal lobar degeneration, stroke and neurologically healthy controls. The grey and white matter from a total of 22

samples, of which 12 were positive for pTDP-43 pathology on viewing the whole slide, were assessed by virtual TMA core(s).

A virtual core or the whole ROI was deemed positive for pathology if two or more phosphorylated-TDP-43 (pTDP-43) inclusions were present in glial cells or neurons or as neurites. A virtual core or whole ROI was deemed negative if one or no inclusions were present within that region.

Three virtual cores measuring 1.75mm diameter were randomly positioned in the grey matter or white matter regions of each image. The sensitivity and specificity of these cores with relation to detecting pTDP-43 pathology was calculated as below.

$$Sensitivity = \frac{True\ positive\ cores}{True\ positive\ cores + False\ negative\ cores} \times 100,$$

$$Specificity = \frac{True\ negative\ cores}{True\ negative\ cores + False\ positive\ cores} \times 100,$$

Following this, sections from the spinal cord at variable levels from eight cases of sporadic MND with varying severity of disease were assessed. The ROIs were the lateral corticospinal tract, dorsal columns and anterior horns. Due to the small size of these structures, only two virtual cores could be achieved.

## 5.5 TMA Construction

TMAs were produced with a total of 33 cores per block. A number of measures were taken to ensure consistent orientation of sections such that the location of individual cores in each block could be reliably determined: Firstly, two cores of chicken breast meat were included in one corner. Secondly, cores were not set out in a rectangular array with rotational symmetry by omitting cores from the final row (**Figure 3**). Workup of the tissue microarray protocol was performed firstly using pig brain obtained from a local abattoir.

The procedure was adapted from a previously established method (Fowler et al., 2011) using a Beecher MTA-1 Tissue Microarrayer. This involves harvesting a number of donor cores (in this case 2mm diameter, *as described in section 5.1)* from appropriate donor blocks, and placement of these in a grid pattern within pre-formed holes created within a recipient paraffin block (**See figure 1**). However, as we were using larger cores than Fowler et al. (2mm), a larger spacing between cores was needed (1mm). The recipient blocks were incubated at 37°C for 15 minutes, prior to the removal of wax cores. This warming enabled slight softening of the paraffin, reducing the force required from the needle when punching into the wax. After heating, all of the 35 required holes within the recipient block were generated before the insertion of donor cores.

Prior to donor core extraction, a Luxol fast blue (LFB) stain was performed to allow differentiation between grey and white matter. Each donor core was 5mm in depth, providing a compromise between adequate tissue for downstream analysis and the probability of fracturing the donor block, which is more common with deeper donor cores. After construction of a complete TMA, the recipient stylet and donor stylet were thoroughly cleaned with xylene.

Cores can 'fall out' of sections (core loss) from a tissue microarray either during sectioning or during staining. To minimise this, an annealing step was added prior to sectioning. This involved heating the completed recipient block repeatedly to 37°C for five, 10-minute intervals. After each 10-minute interval, gentle manual pressure was applied using a microscope slide placed on top of the paraffin block. This allowed the paraffin to mould firmly around each core, with the applied manual pressure acting to 'seat' the cores more securely within the block.

Once the TMAs had been produced, the core loss during processing to a final stained or immunolabelled section was assessed as a function of varying section thickness, slide type and post sectioning incubation. A core was deemed to have been lost when approximately 50% of the tissue was no longer correctly sited on the slide.

Sections were cut at 4µm, 5µm, and 7µm thickness, with the number of cores lost at sectioning recorded across a series of 5 slides for each condition. We also trialled differing microscope slides: Waldemar Knittel Glasbearbeitungs GmbH (Braunschweig, Germany) StarFrost, Trajan Scientific and Medical (Ringwood, Victoria, Australia) Series 1 and 2. Varying incubation times (1hr or overnight) and temperatures (60$^{O}$C or 37$^{O}$C) were assessed for core adherence. CD68 and Iba-1 immunohistochemistry runs were conducted both manually and using an autostainer (see Waller et al., 2019) to assess the impact this would have.

### 5.6 Statistical Analyses

*A variety of statistical analysis was used through this study, the details of which can be found in each relevant section. In summary, for the quantitative measures (microglial), Spearman's Rank Correlation (two-tailed) was used to assess the correlation between the 'gold standard' measures and those from the TMAs. This was used as most data had a non-normal distribution, as per a Kolmogorov-Smirnov goodness of fit test. This was followed by Bland-Altman plots to measure the reliability of one, two or three TMAs (Bland and Altman, 1999; Gagliardi et al., 1992; O'Brien et al., 1993), whilst sensitivity and specificity were calculated for the qualitative assessment (pTDP-43).*

## 6 Results

### 6.1 White Matter Lesion Microglial Quantitative Analysis

A Spearman's rank correlation coefficient showed good correlation between the whole ROI measurements and the mean of three, two or one virtual core measurements of 1.75mm diameter (**Table 1A**; all $\rho \geq 0.839$, all $P<0.001$).

The deviation of a TMA measure from the 'gold standard' measure of the whole ROI, is best viewed in the context both of the spread of values within a group of interest as well as the size of intergroup differences. We thus assessed the size of intergroup differences in the microglial data for the whole ROI. As already described for the larger cohort from which

these data for the current study were drawn (Waller et al., 2019), significant intergroup differences were seen: For area density, Iba-1 had a 60% lower area density in DSCL than controls with NAWM being 37% higher than control and 128% greater than DSCL. The CD68 area density was 366% greater in the DSCL group than controls, whilst NAWM was 36% greater than DSCL. A similar pattern is seen for MHCII, with an increase of 33% from the control to the DSCL group and 63% from the DSCL to the NAWM group. Given that intergroup differences tended to be in the tens of percentage points, we considered it reasonable to assess accuracy in terms of the proportion of data points from virtual cores that lie within 10% of the gold standard whole ROI measure. We wished that 60% or more of measures should lie within this range.

We next assessed bias and reliability of virtual core TMA data using Bland-Altman plots (see **supplementary figure 1**). The full ROI data were used to calculate 'error ranges': Thus, the ±5% and ±10% error ranges were 5% and 10% of the full range of data from the whole ROI. In twelve of these plots, when estimating the range of the whole ROI measurements a clear outlier was noted, which was excluded when estimating the 5% and 10% error range (thereby making the assessment of the virtual core data more stringent). These Bland Altman plots were then used to calculate a ±5% and ±10% accuracy (described above), based on the number of data points falling within 5% and 10% error ranges respectively (**Table 1B**). In brief, the ±5% and ±10% accuracy determine the percentage of TMA measures that fall within the ±5% and ±10% error ranges.

At ±10%, good accuracy was seen: For area density (the proportion of the digital image that was positive for immunostain) for all 3 markers (Iba1, CD68 and MHC-II), there was ≥67% accuracy even when only one virtual core was assessed. There was a slight improvement if the mean of two virtual cores was used. For the average size of microglial profiles, there was 62% accuracy for one core, rising to 77% and 86% for the mean of 2 and 3 virtual cores respectively. For the shape metric, a single virtual core gave poor (38%) accuracy, which was improved by using the mean of 2 cores which achieved (69% accuracy). No consistent

under or over estimation by virtual TMA cores was identifiable. The ±5% accuracy was mostly poor throughout.

Based on these data, it seems reasonable to conclude from this modelling that TMA cores are representative of data from the whole region of interest at the ±10% accuracy level: One such core gives sufficient accuracy for measuring area density, while the mean of 2 cores is needed for measuring the size and shape of microglia on these measures.

## 6.2 Spinal Cord Microglial Quantitative Analysis

In order to explore TMA use for microglial pathology further in another disease process, archival CD68-immunostained sections of spinal cord from cases of MND were studied. The regions of interest were anterior horn, lateral corticospinal tract and dorsal column. Generally, only two virtual cores could be generated due to the small size of these structures. Spearman's rank correlation coefficient, *two-tailed*, was used to assess the correlation between the ROI and the cores. A strong correlation was seen between the whole ROI and the virtual cores across all regions and measurements, both with one virtual core or the mean of two virtual cores were assessed (**Table 2A**).

Bland Altman plots were drawn as for the white matter lesion data (**supplementary figure 2**). For area density, the ±10% error limits gave good accuracy, in all regions being ≥89% for one or the mean of two virtual cores (**Table 2B**). At the more stringent ±5% error limit level, area density measurements still performed well, with accuracy of ≥78% achievable with only one core. The profile size and shape metrics were also reasonable with ±10% error limits: for the shape metric, ≥78% accuracy could be achieved with one core alone. For average microglial profile size, a mean of two cores was necessary for the dorsal columns to achieve 63% accuracy as using a single core only gave 56% accuracy.

Taking these spinal cord and deep white matter data together and in the context of detecting differences in the order of tens of percentage points, it would appear that good, accurate measures of area volume may be achieved with a single TMA core of around 2mm diameter.

Greater numbers of core sections are needed for more sophisticated profile size and shape order measures.

## 6.3 Cortical Quantitative Assessment of Microglia in MND

In order to assess the effectiveness of TMA measurement of microglial pathology in a further CNS region, we examined archival CD68-immunolabelled slides from the cortex. These included seven cortex sections from MND cases, three frontal cortex sections from MND cases and three sections of cortex from cases with white matter lesions but without MND or frontotemporal lobar degeneration. As in both the WM and spinal cord analysis, a strong Spearman's rank correlation was seen between the whole ROI measurements and the 1.75mm virtual core measurements for area density, even when only one virtual core is utilised (**Table 3A**). The correlation is reduced but still strong for the profile size measurements, though a clear improvement is seen here with the use of an average of two virtual cores compared to one virtual core. For the shape metric measurements, an unexpected pattern is seen with the measurements taken from one virtual core showing the greatest correlation.

Following this, Bland-Altmann plots were produced as before (**Table 3B**). No obvious bias (over or under estimation) from virtual core assessment compared to the whole ROI were seen. There was reasonable accuracy when measuring area density at ±10% accuracy (ranging from ≥67% for a single core to ≥79% for the mean of 3 cores. When ±5% accuracy was considered, good accuracy could not be reliably achieved, in some cases even with 3 cores. For profile size and shape measures, reasonable accuracy was possible at ±10%, albeit with the mean of 2 measures necessary for shape, whilst adequate ±5% accuracy was difficult to achieve.

Having assessed the ability of TMAs to assess microglial pathology in a number of CNS regions in a number of settings we drew the following conclusions:

At the ±10% level, reasonable estimates of area density could be achieved with a 2mm TMA cores with a single core. However, greater numbers of cores were required to assess more complex features such as profile size and shape. These TMAs were not sufficiently accurate at the ±5% level.

## 6.4 pTDP-43 Cortex and Spinal Qualitative Analysis

Having established the feasibility of using TMAs to assess quantitative neuropathological measures (microglial markers in this instance), we wished to consider TMA use in the context of qualitative assessments: ie, the achievable sensitivity and specificity for detecting TDP-43 proteinopathy.

The presence of at least two pTDP-43 aggregates within the examined area was set as the criterion for classifying a sample positive for TDP-43 proteinopathy. The virtual TMA core data were compared to the whole ROI in the digitised image as the 'gold standard' to calculate sensitivity and specificity (**Table 4**).

In the forebrain, the sensitivity and specificity for the grey matter (GM) were 100%, irrespective of how many cores were used to assess pathology. The specificity score for WM (where pTDP-43 pathology is sparser than GM) was 100%, but sensitivity scores were more varied at 88.33%, 97.09% and 100% for 1, 2 and 3 cores respectively.

The spinal cord yielded a sensitivity of 100% in the anterior horns with just a single virtual core. Specificity was not tested, as all full ROIs were positive for pathology. For the corticospinal tract, the sensitivity was 58% and 76% for one and two virtual cores respectively and the specificity was 66.67% for both one and two virtual cores. In the dorsal columns, there was poor sensitivity (8.34% and 16.67% for one and two virtual cores respectively), but better specificity (96.34% and 92.86% for one and two pooled cores).

We conclude from this that TMAs can be used to make qualitative assessments of the presence or absence of inclusion bodies in situations where pathology has a reasonable density when present, such as TDP-43 proteinopathy in the grey matter in MND. Where

pathological features are sparser, as is the case for TDP-43 proteinopathy in the white matter in MND, this is less feasible. More specifically, a single core is adequate to assess the presence vs absence of phosphorylated TDP-43 inclusions in grey matter structures.

## 6.5 TMA Optimisation

We next wished to generate a protocol for construction of TMAs of 2mm core diameter from with post mortem brain tissue. TMAs were constructed using a Beecher MTA-1 Tissue Microarrayer.

We found that incubating recipient and donor blocks at 37°C for 15 minutes prior to use prevented both block types fracturing during core extraction and placement. Stylets had to be regularly cleaned to remove paraffin build up. A 33 core TMA could be constructed in 1.5 hours or less.

An annealing step post construction is key for maintaining TMA integrity. This involves repeated (5 cycles) heating of the recipient block after all cores had been placed at 37°C for 10 minutes. After each 10-minute interval is completed, gentle manual pressure is applied to the top of the TMA block with a microscope slide. This softens the paraffin and moulds it around the donor cores, preventing ‘core loss’ during sectioning.

Having constructed the TMA, a key issue to address is core loss. This can happen due to 1) cores to ‘dropping out’ from the section when it is cut and 2) cores becoming detached from the microscope slide during staining.

We first examined whether varying section thickness could decrease core loss from 33 core TMAs. With respect to core drop-out at sectioning, there was little difference between 5µm (mean of 1.58 cores out of 33/5.8% lost) and 7µm (mean 1.66 of 33/5.0% lost) sections. However, on staining by haematoxylin and eosin; H&E, there was lesser core loss in the 5µm sections (mean 12.33 of 33/37.4% lost) than the 7µm sections (mean 17 of 33/51.5% lost). Therefore, the ideal thickness at which to section each TMA was 5µm.

Core adherence at staining was improved by incubating the slides at 37°C overnight followed by a 1-hour incubation at 60°C prior to staining, reducing core loss to 2.2 out of 33 (6.7%).

Further improvements were brought about using slides with more advanced adhesive coatings. Thus, Trajan Series 1 and 2 demonstrated reduced mean core loss of 0.8 and 0.6 out of 33 (2.4% and 1.8%) cores lost respectively.

Our protocol thus far was to cut sections at 5µm section thickness, mount on Trajan slides and incubate at 37°C overnight followed by a 1-hour at 60°C.

Having optimised core section retention for H&E, we proceeded to trial immunostaining for CD68 and Iba1 both manually and by autostainer. There was no discernible difference in core loss between H&E staining (as above) and immunostaining either manually or by autostainer. The average loss out of 33 cores for manual staining of CD68 and Iba-1 was 0.66 (2.0%) and 0.5 (1.5%) respectively, compared to the autostainer loss of 0.66 (2.0%) and 0.75 (2.3%).

We also found that performing a luxol fast blue-stained section of each donor block helps to determine its architecture. However, there may still instances where the resultant TMA cores were ‘off target’ (e.g. sampling white matter instead of cortex) due to the three-dimensional nature of tissue, such that the surface of the block is not always a good indicator of the underlying tissue. In order to limit this, we advise that cores should be extracted from as far away from tissue boundaries as possible.

# 7 Discussion

We aimed to establish if tissue microarrays (TMAs) could be used to assess post mortem neuropathology. Firstly, we investigated the degree to which microscopy of the relatively small core section could represent data from larger, whole block sections. We then

established a protocol for creating and sectioning TMA blocks to maximise core section retention for neurohistology.

The concordance of core sections was first investigated with respect to microglial immunohistochemistry (a quantitative measure) in two scenarios: Deep white matter lesions in the ageing brain and the brain and spinal cord in MND. Additionally, concordance for qualitative assessments of inclusion pathology was assessed for phosphorylated TDP-43 inclusions in MND.

We determined that microglial pathology can be reliably represented by TMAs in both white matter lesions and MND and that TDP-43 pathology can be reliably assessed with TMA cores. We developed optimised conditions in which to construct TMAs.

For the microglial measures of white matter lesions, there was a strong correlation between data from single virtual cores and whole regions of interest (ROIs). Further assessment with Bland-Altman plots gave a more accurate assessment of relationships between two measures (Bland and Altman, 1999). This is a well-established method for assessing the accuracy of medical quantitation systems. In the context of TMAs, this method has previously been used to evaluate differences between different size cores in surgical pathology neoplasia samples (Karlsson et al., 2009) but not to calculate differences between a 'gold standard' whole ROI and 'virtual' cores in post mortem neuropathology. *The use of Bland-Altman plots in this context allow assessment across the whole data range, with exclusion of obvious outliers to increase stringency. This allows incorporation of the various pathology densities experienced with Iba-1, CD68 and MHCII into their own individual accuracy measures.*

These Bland-Altman plots from WM comparisons demonstrated good accuracy using just a single core for basic area density of microglial burden, whilst more sophisticated measures (profile size or shape) required taking the mean of two virtual cores. This degree of accuracy is reasonable when viewed in the context of the size of intergroup differences (which ranged

in our data from 33% to 366%). This is similar to the number of cores used previously in oncological studies, with two 2mm cores and three 3mm cores used commonly (Gillett et al., 2000; Hoos and Cordon-Cardo, 2001). In the small number of neuropathology studies so far, the number of cores used can vary from one (Alafuzoff et al., 2008) to two or more (Martikainen et al., 2006; Walker et al., 2017). In comparison to this, using two 2mm cores would allow a reduction in tissue usage.

In the spinal cord, similar to the white matter lesions, a good correlation was seen between the whole ROI measurements and those from one virtual core. Bland Altman plots of CD68-immunostained spinal cord sections demonstrated a high accuracy of area density could be achieved with one core. Again, shape metric measures and profile size required more cores or sections: a mean of two for shape and probably more for profile size. Inevitably, the number of cores and thus accuracy needs to be adapted in the light of the effect size that any investigation is attempting to detect.

In the neocortex of MND cases, TMAs managed to give reasonable accuracy with a single virtual core for area density of microglial staining. Again, more cores were required for more sophisticated measures of profile size and shape.

The assessment of pTDP-43 within MND spinal cord sections revealed a good sensitivity and specificity when using one core for grey matter and two for white matter: Within grey matter sensitivity and specificity were consistently 100%, irrespective of the number of cores analysed. Similarly, specificity for white matter regions was 100% for 1-3 cores. However, sensitivity was lower in white matter regions as the pathology in this region was less dense when compared to grey matter.

For the spinal cord regions, the pTDP-43 status of the anterior horns can be accurately represented using one core, whereas for the corticospinal tract, two cores allow a greater accuracy. If the dorsal columns are to be assessed, two cores should be used to gain a reasonable specificity whilst a reasonable sensitivity is unattainable using two cores. This

may be due to non-specific tissue incorporation in these cores, due to overlap with adjacent areas.

Stylets should be frequently cleaned and recipient and donor blocks should be incubated at 37°C for 15 minutes prior to use. When donor blocks are readily available, 33 core TMAs could be constructed in 1.5 hours or less. Although this initial construction phase may appear time consuming, it allows the generation of a block comprising 33 different samples, proving less time consuming than taking whole sections from donor blocks where a large cohort is required (Martikainen et al., 2006).

Cores should be taken from the centre of the region of interest, away from interfaces with other tissue types, to minimise the tendency for off-target sampling in deeper levels within the core. *A section thickness of 5µm collected on microscope slides with advanced adhesive coated slides, with both an overnight incubation at 37$^{O}$C and further incubation of one hour at 60$^{O}$C immediately prior to staining to minimise core loss is recommended*. In our hands, this gave an average loss of 1.8% cores. This is similar to previous work which had core loss of 1% - 2% (Horvath and Henshall, 2001) and 2.7% - 3.7% (Martikainen et al., 2006), although other studies with different protocols have had greater core loss, ranging from 10% to 37% (Hoos and Cordon-Cardo, 2001). Furthermore, there was little fracturing of the block seen with 2mm cores, compared to that reported previously (Sjöbeck et al., 2003), possibly due to our practice of pre warming the TMA block.

Limiting the core depth to 5mm core depth may have reduced block fracture and preserved tissue from deeper in the block.

It is inevitable that the smaller sample present in a TMA core will give less accurate measures than when a full region of interest is sampled. However, this has to be viewed in the light of the greater number of cases that can be assessed given finite time and resources. Thus, there is a simultaneous increase in sampling at the level of the study comparison group at the same time as reduced sampling at the level of the individual. It is

thus necessary for any neuropathological study to determine whether this compromise is acceptable.

We cannot study all possible measures of all possible disease conditions, so our conclusions that TMAs can be used in post mortem neuropathology may not be infinitely generalizable. However, we have looked at two types of measure in two disease processes in an attempt to address this and hope that the study presented here, together with other studies in the literature, will usefully inform scientists wishing to use TMAs in this manner. This study adds to a small but growing literature that demonstrates the feasibility of using this technology in neurodegenerative post mortem research studies (Alafuzoff et al., 2008; Martikainen et al., 2006; Walker et al., 2017).

Finally, after a TMA has been made there is a core missing from every level of the donor block. Ideally, only cases with large sized or numerous donor blocks should be used, such that if a larger, conventional section is required from the donor block for future studies, this remains possible after sampling.

# 8 Acknowledgements

This work has been supported by the OCEAN project (EP/M006328/1) funded by the Engineering and Physical Sciences Research Council (EPSRC). We are grateful to our respondents and their families for their generous gift to medical research, which has made this study possible. The Nanozoomer XR scanner was funded by the bet365/Denise Coates Foundation.

BA is supported by a PhD studentship from the Pathological Society of Great Britain and Ireland.

We are grateful to the Sheffield Brain Tissue Bank for the provision of MND tissue.

We would like to thank the individuals who have donated tissues for research and to their next of kin who have assisted with this.

# 9 Figures

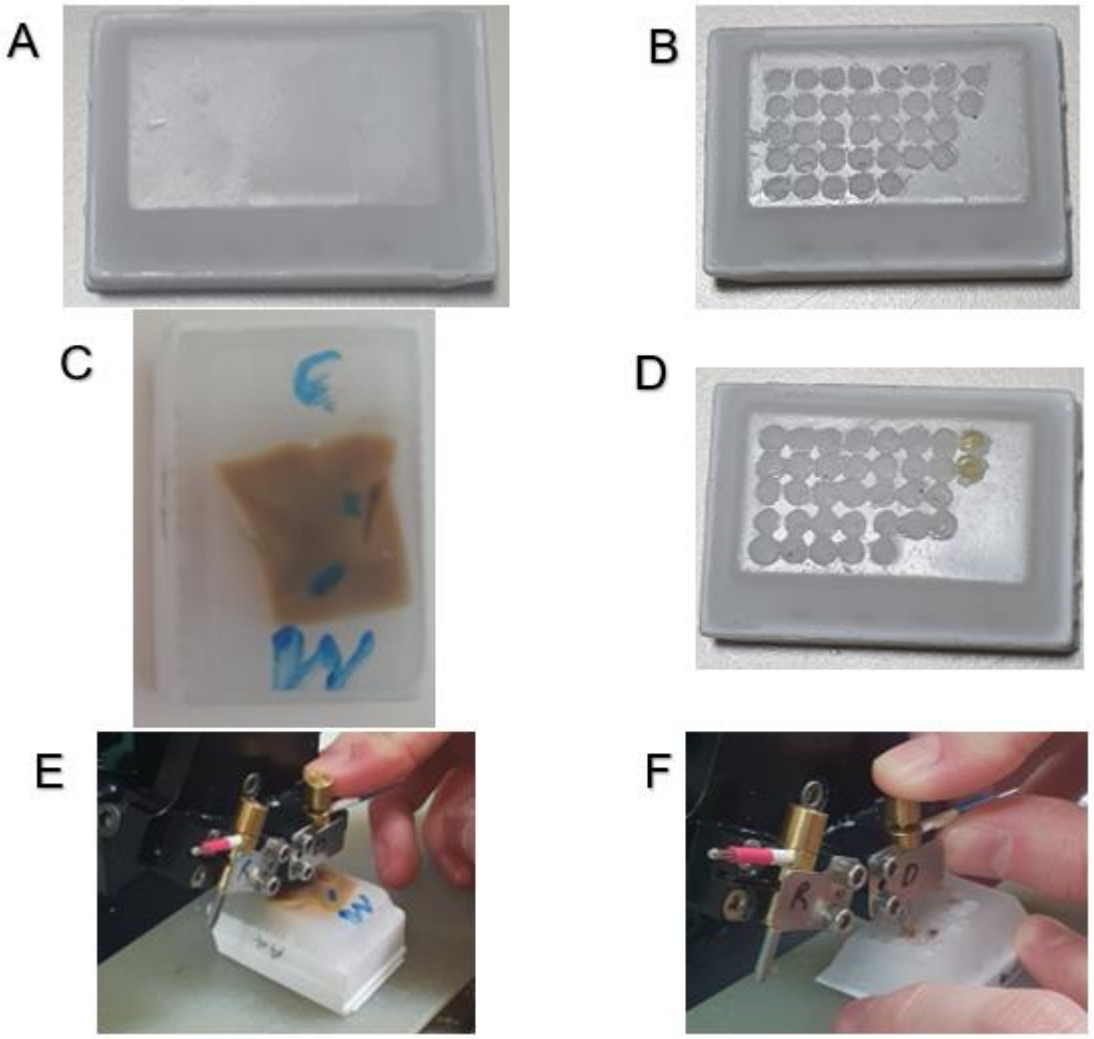


**Figure 1**: *Construction of a TMA*: (A) The recipient stylet is inserted into a blank paraffin block, extracting paraffin cores resulting in the creation of a recipient block (B). (C) A 'donor block' is selected, and target areas identified (in this case grey and white matter labelled G and W respectively). From each target area, a 2mm core is removed via the donor stylet (E), which is placed into the corresponding hole of the 'recipient block' (F).

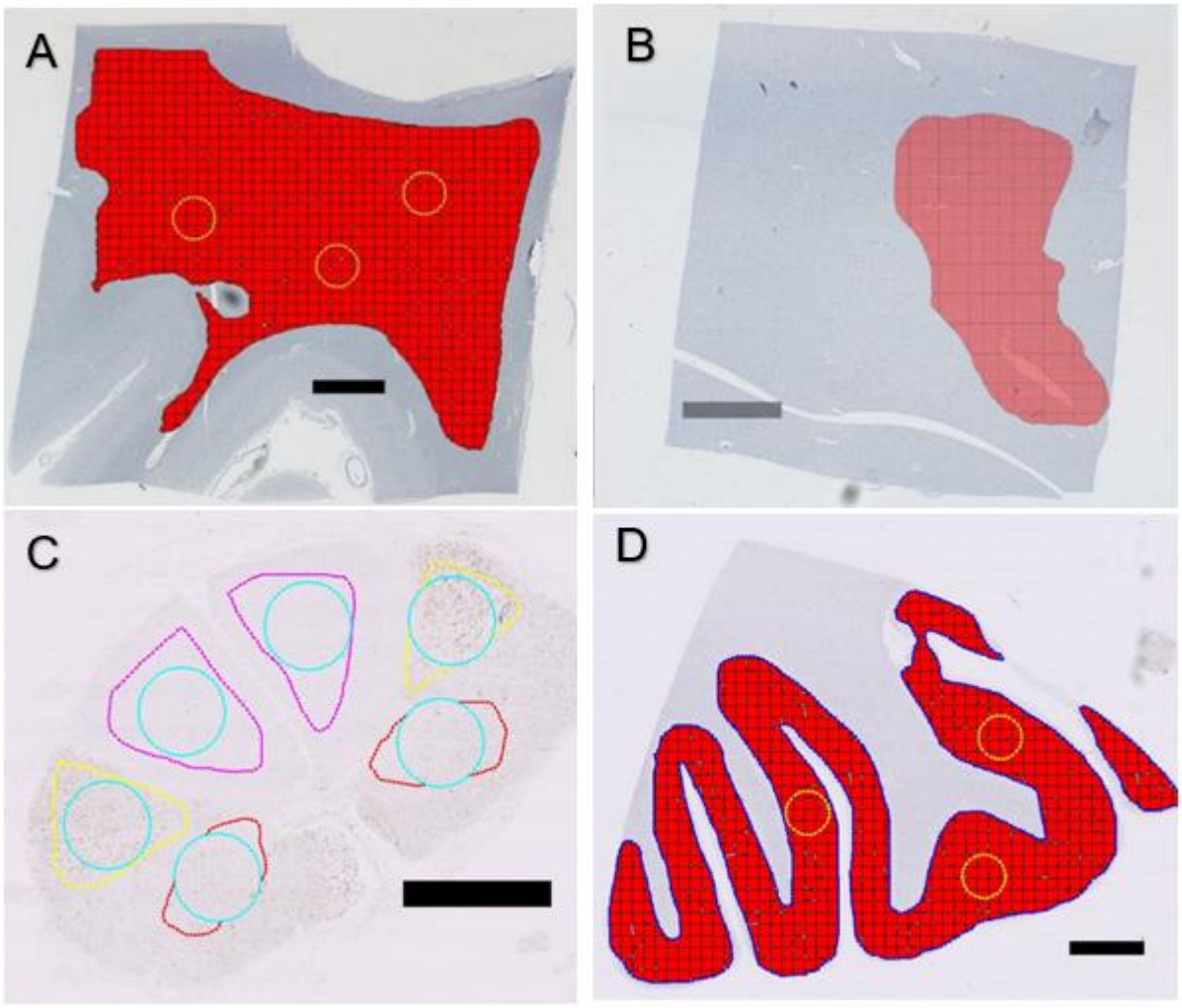


**Figure 2:** *Regions of interest (ROIs) and placement of virtual cores:* (A) The red area represents the area identified as the whole ROI (in this case the full extent of the white matter, excluding artefactual changes. Overlaid in yellow are the random positioning of the virtual cores within this area. (B) The red area highlights the whole region of interest in another case (a deep subcortical lesion) with the ROI consisting of the extent of microglial activation. (C) The ROIs highlighted in this image correspond to the anterior horn (outlined in red), the lateral corticospinal tracts (outlined in yellow) and the dorsal columns (outlined in purple). Within each ROI, outlined in blue, is the location of each virtual core. (D) Highlighted in red is the extent of the whole ROI, with the positioning of the virtual cores outlined in yellow. Scale bar 3mm.

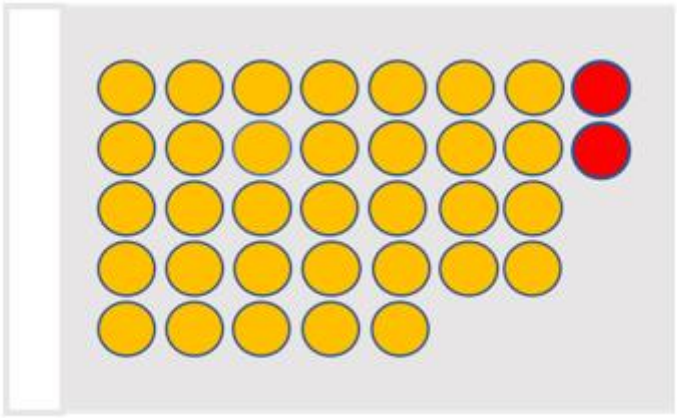

**Figure 3:** *Diagrammatic representation of the **l**ayout of tissue microarray cores within the recipient block.* The yellow circles represent tissue TMA cores, harvested from the 'donor block' and placed within pre-formed holes in the 'recipient block.' The last row has two spaces omitted to minimise rotational symmetry. The two red circles represent chicken muscle, which are used to further aid orientation.

# 10 Tables

## A

| Number of Cores Compared to Whole ROI | Spearman's Correlation Coefficient Results – White Matter Microglial Lesion Concordance | | | | | |
|---|---|---|---|---|---|---|
| | Area Density | | Average Size | | Shape Metric | |
| | Correlation | Sig | Correlation | Sig | Correlation | Sig |
| **3** | 0.977 | <0.001 | 0.918 | <0.001 | 0.957 | <0.001 |
| **2** | 0.964 | <0.001 | 0.882 | <0.001 | 0.839 | <0.001 |
| **1** | 0.964 | <0.001 | 0.904 | <0.001 | 0.911 | <0.001 |

## B

| Bland-Altman Accuracy Results – White Matter Microglial Lesion Concordance | | | | |
|---|---|---|---|---|
| **Measurement** | **Immunostain** | **Number of Cores** | **±10% Accuracy** | **±5% Accuracy** |
| **Area Density** | **Iba-1** | 3 | 86.67% | 80.00% |
| | | 2 | 66.67% | 53.33% |
| | | 1 | 66.67% | 46.67% |
| | **CD68** | 3 | 85.71% | 92.86% |
| | | 2 | 92.31% | 61.54% |
| | | 1 | 69.23% | 53.85% |
| | **MHCII** | 3 | 78.57% | 28.57% |
| | | 2 | 71.43% | 28.57% |
| | | 1 | 71.43% | 14.29% |
| **Average Size** | **CD68** | 3 | 85.71% | 57.14% |
| | | 2 | 76.92% | 38.46% |
| | | 1 | 61.54% | 53.85% |
| **Shape Metric** | **CD68** | 3 | 71.43% | 35.71% |
| | | 2 | 69.23% | 46.15% |
| | | 1 | 38.46% | 30.77% |

**Table 1:** *Results from correlation and Bland-Altman analysis of concordance between a whole region of interest and 1.75mm diameter virtual cores of immunolabelled white matter.* (A) Spearman's correlation, two-tailed, results for varying numbers of virtual cores compared to a whole ROI following WM lesion concordance analysis. The 'correlation' refers to the correlation co-efficient ($\rho$) and the 'Sig' refers to the significance (p-value). (B) Bland-Altman measures of white matter microglial lesion concordance using varying numbers of virtual cores compared to a whole ROI. The ±10% or ±5% accuracy was calculated based on the proportion of data points, excluding any outliers, lying within the 10% or 5% error range of a non-parametric Bland Altman plot.

**A**

| Number of Cores Compared to Whole ROI | Spearman's Rank Correlations – Lateral Corticospinal Tract Microglial Lesion Concordance | | | | | |
|---|---|---|---|---|---|---|
| | Area Density | | Average Size | | Shape Metric | |
| | Correlation | Sig | Correlation | Sig | Correlation | Sig |
| **2** | 0.993 | <0.001 | 0.933 | <0.001 | 0.986 | <0.001 |
| **1** | 0.984 | <0.001 | 0.889 | <0.001 | 0.874 | <0.001 |

**B**

| Number of Cores Compared to Whole ROI | Spearman's Rank Correlations – Dorsal Columns Microglial Lesion Concordance | | | | | |
|---|---|---|---|---|---|---|
| | Area Density | | Average Size | | Shape Metric | |
| | Correlation | Sig | Correlation | Sig | Correlation | Sig |
| **2** | 0.986 | <0.001 | 0.818 | <0.001 | 0.946 | <0.001 |
| **1** | 0.989 | <0.001 | 0.777 | <0.001 | 0.928 | <0.001 |

**C**

| Number of Cores Compared to Whole ROI | Spearman's Rank Correlations – Anterior Horn Microglial Lesion Concordance | | | | | |
|---|---|---|---|---|---|---|
| | Area Density | | Average Size | | Shape Metric | |
| | Correlation | Sig | Correlation | Sig | Correlation | Sig |
| **2** | 0.991 | <0.001 | 0.877 | <0.001 | 0.982 | <0.001 |
| **1** | 0.991 | <0.001 | 0.835 | <0.001 | 0.972 | <0.001 |

**D**

| Bland Altman Accuracy Results from Spinal Cord Microglial Lesion Concordance | | | | |
|---|---|---|---|---|
| **Measurement** | **Area Assessed** | **Number of Cores** | **±10% accuracy** | **±5% accuracy** |
| **Area Density** | **Corticospinal Tracts** | 2 | 100% | 94.44% |
| | | 1 | 94.11% | 82.35% |
| | **Dorsal Columns** | 2 | 100% | 88.24% |
| | | 1 | 100% | 88.24% |
| | **Anterior Horns** | 2 | 88.89% | 83.33% |
| | | 1 | 88.89% | 72.22% |
| **Average Size** | **Corticospinal Tracts** | 2 | 94.12% | 82.35% |
| | | 1 | 61.11% | 44.44% |
| | **Dorsal Columns** | 2 | 62.50% | 56.25% |
| | | 1 | 56.25% | 31.25% |
| | **Anterior Horns** | 2 | 77.78% | 61.11% |
| | | 1 | 83.33% | 61.11% |
| **Shape Metric** | **Corticospinal Tracts** | 2 | 100% | 94.74% |
| | | 1 | 84.21% | 73.68% |
| | **Dorsal Columns** | 2 | 94.44% | 83.33% |
| | | 1 | 94.44% | 55.56% |
| | **Anterior Horns** | 2 | 83.33% | 77.78% |
| | | 1 | 77.78% | 61.11% |

**Table 2:** *Results from correlation and Bland-Altman analysis of concordance between a whole region of interest and 1.75mm diameter virtual cores of CD68 immunolabelled spinal cord. (A, B and C)* Spearman's Correlations, *two-tailed*, of microglial lesion concordance from the mean of two or one virtual cores compared to the whole ROI for each region (lateral corticospinal tract, dorsal column and anterior horn). Correlation refers to Spearman's $\rho$ 'sig' to P. (D) Bland Altman accuracy results of microglial lesion concordance in varying areas of the spinal cord. The ±10% and ±5% accuracy was calculated as the proportion of data points within the 10% and 5% error range respectively.

**A**

| Spearman's Correlation Results - Cortical Microglial Lesion Concordance | | | | | | |
|---|---|---|---|---|---|---|
| **Number of Cores Compared to Whole ROI** | **Shape Metric** | | **Average Size** | | **Area Density** | |
| | **Correlation** | **Sig** | **Correlation** | **Sig** | **Correlation** | **Sig** |
| **3** | 0.780 | 0.002 | 0.918 | <0.001 | 0.978 | <0.001 |
| **2** | 0.714 | 0.006 | 0.868 | <0.001 | 0.973 | <0.001 |
| **1** | 0.852 | <0.001 | 0.769 | 0.002 | 0.967 | <0.001 |

**B**

| Bland Altman Accuracy Results – Cortical Microglial Lesion Concordance | | | |
|---|---|---|---|
| **Measurement** | **Number of Cores Compared to Whole ROI** | **±10% accuracy** | **±5% accuracy** |
| **Area Density** | **3** | 84.6154 | 61.5385 |
| | **2** | 76.9231 | 61.5385 |
| | **1** | 84.6154 | 61.5385 |
| **Average Size** | **3** | 76.9231 | 53.8462 |
| | **2** | 69.2308 | 53.8462 |
| | **1** | 46.1538 | 46.1538 |
| **Shape Metric** | **3** | 53.8462 | 30.7692 |
| | **2** | 38.4615 | 15.3846 |
| | **1** | 61.5385 | 38.4615 |

**Table 3:** *Results from correlation and Bland-Altman analysis of concordance between a whole region of interest and 1.75mm diameter virtual cores of CD68 immunolabelled cortex.* (A) Spearman's correlation, *two-tailed*, results for varying numbers of virtual cores compared to a whole ROI following cortical lesion concordance analysis. The 'correlation' refers to the correlation co-efficient ($\rho$) and the 'Sig' refers to the significance (p-value). (B) Bland-Altman measures of cortical microglial lesion concordance using varying numbers of virtual cores compared to a whole ROI. The ±10% or ±5% accuracy was calculated based on the proportion of data points, excluding any outliers, lying within the 10% or 5% error range of a non-parametric Bland Altman plot.

**A**

| TDP-43 Status Concordance Results - Cortex | | | | | | |
|---|---|---|---|---|---|---|
| **Region** | **Grey Matter** | | | **White Matter** | | |
| **Number of Cores Compared to Whole ROI** | 1 | 2 | 3 | 1 | 2 | 3 |
| **Sensitivity** | 100% | 100% | 100% | 88.33% | 97.09% | 100% |
| **Specificity** | 100% | 100% | 100% | 100% | 100% | 100% |

**B**

| TDP-43 Status Concordance Results – Spinal Cord (Individual Cores) | | | | | | |
|---|---|---|---|---|---|---|
| **Region** | **Corticospinal Tract** | | **Dorsal Columns** | | **Anterior Horns** | |
| **Core Position** | **Right** | **Left** | **Right** | **Left** | **Right** | **Left** |
| **Sensitivity** | 62.50% | 52.94% | 16.67% | 0.00% | 100.00% | 100.00% |
| **Specificity** | 66.67% | 66.67% | 92.86% | 100.00% | N/A | N/A |

**C**

| TDP-43 Status Concordance Results – Spinal Cord (Pooled Cores) | | | |
|---|---|---|---|
| **Region** | **Corticospinal Tract** | **Dorsal Columns** | **Anterior Horns** |
| | **Pooled Cores** | **Pooled Cores** | **Pooled Cores** |
| **Sensitivity** | 76.47% | 16.67% | 100.00% |
| **Specificity** | 66.67% | 92.86% | N/A |

**Table 4:** *pTDP-43 concordance assessment via sensitivity and specificity of varying numbers of virtual 1.75mm diameter cores compared to the whole ROI in cortical and spinal cord regions*. (A) Sensitivity and specificity for one core, two cores and three cores within the grey matter and white matter. (B) The calculated sensitivity of the concordance of pTDP-43 status within the spinal cord using a single virtual core (B) and pooling two cores (C).

**References:**


Alafuzoff, I., Pikkarainen, M., Arzberger, T., Thal, D.R., Al-Sarraj, S., Bell, J., Bodi, I., Budka, H., Capetillo-Zarate, E., Ferrer, I., Gelpi, E., Gentleman, S., Giaccone, G., Kavantzas, N., King, A., Korkolopoulou, P., Kovács, G.G., Meyronet, D., Monoranu, C., Parchi, P., Patsouris, E., Roggendorf, W., Stadelmann, C., Streichenberger, N., Tagliavini, F., Kretzschmar, H., 2008. Inter-laboratory comparison of neuropathological assessments of β-amyloid protein: A study of the BrainNet Europe consortium. Acta Neuropathol. 115, 533–546. https://doi.org/10.1007/s00401-008-0358-2

Altman, D.G., Bland, J.M., 1983. Measurement in Medicine: the Analysis of Method Comparison Studies. Stat. 32, 307–317.

Arai, T., Hasegawa, M., Akiyama, H., Ikeda, K., Nonaka, T., Mori, H., Mann, D., Tsuchiya, K., Yoshida, M., Hashizume, Y., Oda, T., 2006. TDP-43 is a component of ubiquitin-positive tau-negative inclusions in frontotemporal lobar degeneration and amyotrophic lateral sclerosis. Biochem. Biophys. Res. Commun. 351, 602–611. https://doi.org/10.1016/j.bbrc.2006.10.093

Ashford, B.A., Boche, D., Cooper-Knock, J., Heath, P.R., Simpson, J.E., Highley, J.R., 2020. Review: Microglia in motor neuron disease. Neuropathol. Appl. Neurobiol. https://doi.org/10.1111/nan.12640

Battifora, H., 1986. The multitumor (sausage) tissue block: novel method for immunohistochemical antibody testing. Lab. Invest. 55, 244–248.

Bland, J.M., Altman, D.G., 1999. Measuring agreement in method comparison studies. Stat. Methods Med. Res. 8, 135–160. https://doi.org/10.1177/096228029900800204

Boche, D., Perry, V.H., Nicoll, J.A.R., 2013. Review: Activation patterns of microglia and their identification in the human brain. Neuropathol. Appl. Neurobiol. https://doi.org/10.1111/nan.12011

Boulagnon-Rombi, C., Fleury, C., Fichel, C., Lefour, S., Bressenot, A.M., Gauchotte, G., 2017. Immunohistochemical approach to the differential diagnosis of meningiomas and their mimics. J. Neuropathol. Exp. Neurol. 76, 289–298. https://doi.org/10.1093/jnen/nlx008

Brooks, B.R., Miller, R.G., Swash, M., Munsat, T.L., 2000. El Escorial revisited: Revised criteria for the diagnosis of amyotrophic lateral sclerosis. Amyotroph. Lateral Scler. 1, 293–299. https://doi.org/10.1080/146608200300079536

Coelho, S., Pozo, J.M., Costantini, M., Highley, J.R., Mozumder, M., Simpson, J.E., Ince, P.G., Frangi, A.F., 2018. Local volume fraction distributions of axons, astrocytes, and myelin in deep subcortical white matter. Neuroimage 179, 275–287. https://doi.org/10.1016/j.neuroimage.2018.06.040

De Leeuw, F.-E., De Groot, J.C., Achten, E., Oudkerk, M., Ramos, P., Heijboer, R., Hofman, A., Jolles, J., Van Gijn, J., Breteler, M.M.B., Ramos, L.M.P., Breteler, M.B., 2001. Prevalence of cerebral white matter lesions in elderly people: a population based magnetic resonance imaging study. The Rotterdam Scan Study. J Neurol Neurosurg Psychiatry 70, 9–14. https://doi.org/10.1136/jnnp.70.1.9

Fernando, M.S., Simpson, J.E., Matthews, F., Brayne, C., Lewis, C.E., Barber, R., Kalaria, R.N., Forster, G., Esteves, F., Wharton, S.B., Shaw, P.J., O'Brien, J.T., Ince, P.G., 2006. White matter lesions in an unselected cohort of the elderly: Molecular pathology suggests origin from chronic hypoperfusion injury. Stroke 37, 1391–1398. https://doi.org/10.1161/01.STR.0000221308.94473.14

Fowler, C.B., Man, Y.G., Zhang, S., O'Leary, T.J., Mason, J.T., Cunningham, R.E., 2011. Tissue microarrays: construction and uses. Methods Mol. Biol. 724, 23–35. https://doi.org/10.1007/978-1-61779-055-3_2

Gagliardi, L., Scimone, F., DelPrete, A., Petecca, C., Stival, G., Pasinetti, G., Teani, M., Bianchi, P., Marani, M., Duca, P.G., 1992. Precision of gestational age assessment in the neonate. Acta Pædiatrica 81, 95–99. https://doi.org/10.1111/j.1651-2227.1992.tb12181.x

Gillett, C.E., Springall, R.J., Barnes, D.M., Hanby, A.M., 2000. Multiple tissue core arrays in histopathology research: A validation study. J. Pathol. 192, 549–553. https://doi.org/10.1002/1096-9896(2000)9999:9999<::AID-PATH721>3.0.CO;2-0

Goldstine, J., Seligson, D.B., Beizai, P., Miyata, H., Vinters, H. V., 2002. Tissue Microarrays in the Study of Non-Neoplastic Disease of the Nervous System. J. Neuropathol. Exp. Neurol. 61, 653–662. https://doi.org/10.1093/jnen/61.8.653

Hainsworth, A.H., Minett, T., Andoh, J., Forster, G., Bhide, I., Barrick, T.R., Elderfield, K., Jeevahan, J., Markus, H.S., Bridges, L.R., 2017. Neuropathology of white matter lesions, blood-brain barrier dysfunction, and dementia. Stroke 48, 2799–2804. https://doi.org/10.1161/STROKEAHA.117.018101

Hoersholm-Denmark, 2017. Visiopharm Software. Visiopharm.

Hoos, A., Cordon-Cardo, C., 2001. Tissue microarray profiling of cancer specimens and cell lines: Opportunities and limitations. Lab. Investig. https://doi.org/10.1038/labinvest.3780347

Ince, P.G., Highley, J.R., Kirby, J., Wharton, S.B., Takahashi, H., Strong, M.J., Shaw, P.J., 2011. Molecular pathology and genetic advances in amyotrophic lateral sclerosis: An emerging molecular pathway and the significance of glial pathology. Acta Neuropathol. https://doi.org/10.1007/s00401-011-0913-0

Karlsson, C., Bodin, L., Piehl-Aulin, K., Karlsson, M.G., 2009. Tissue microarray validation: A methodologic study with special reference to lung cancer. Cancer Epidemiol. Biomarkers Prev. 18, 2014–2021. https://doi.org/10.1158/1055-9965.EPI-08-0743

Kononen, J., Bubendorf, L., Kallioniemi, A., Bärlund, M., Schraml, P., Leighton, S., Torhorst, J., Mihatsch, M.J., Sauter, G., Kallioniemi, O.P., 1998. Tissue microarrays for high-throughput molecular profiling of tumor specimens. Nat. Med. 4, 844–847. https://doi.org/10.1038/nm0798-844

Kovacs, G.G., 2019. Molecular pathology of neurodegenerative diseases: Principles and practice. J. Clin. Pathol. https://doi.org/10.1136/jclinpath-2019-205952

Lasiene, J., Yamanaka, K., 2011. Glial cells in amyotrophic lateral sclerosis. Neurol. Res. Int. https://doi.org/10.1155/2011/718987

Malaspina, A., Puentes, F., Amor, S., 2015. Disease origin and progression in amyotrophic lateral sclerosis: An immunology perspective. Int. Immunol. 27, 117–129. https://doi.org/10.1093/intimm/dxu099

Martikainen, P., Louhelainen, A.M., Kauppinen, T., Alafuzoff, I., 2006. Human brain tissue microarrays as a platform to investigate diseases of the nervous system. Brain Res. 1089, 33–43. https://doi.org/10.1016/j.brainres.2006.03.044

Neumann, M., Sampathu, D.M., Kwong, L.K., Truax, A.C., Micsenyi, M.C., Chou, T.T., Bruce, J., Schuck, T., Grossman, M., Clark, C.M., McCluskey, L.F., Miller, B.L., Masliah, E., Mackenzie, I.R., Feldman, H., Feiden, W., Kretzschmar, H.A., Trojanowski, J.Q., Lee, V.M.Y., 2006. Ubiquitinated TDP-43 in frontotemporal lobar degeneration

and amyotrophic lateral sclerosis. Science (80-. ). 314, 130–133. https://doi.org/10.1126/science.1134108

O'Brien, E., Petrie, J., Littler, W., Swiet, M. De, Padfield, P.L., Altman, D.G., Bland, M., Coats, A., Atkins, N., 1993. Short report: An outline of the revised british hypertension society protocol for the evaluation of blood pressure measuring devices. J. Hypertens. 11, 677–679. https://doi.org/10.1097/00004872-199306000-00013

Prins, M.J.D., Ruurda, J.P., Van Diest, P.J., Van Hillegersberg, R., Ten Kate, F.J.W., 2014. Evaluation of the HER2 amplification status in oesophageal adenocarcinoma by conventional and automated FISH: A tissue microarray study. J. Clin. Pathol. 67, 26–32. https://doi.org/10.1136/jclinpath-2013-201570

Prins, N.D., Scheltens, P., 2015. White matter hyperintensities, cognitive impairment and dementia: An update. Nat. Rev. Neurol. https://doi.org/10.1038/nrneurol.2015.10

Renton, A.E., Chiò, A., Traynor, B.J., 2014. State of play in amyotrophic lateral sclerosis genetics. Nat. Neurosci. https://doi.org/10.1038/nn.3584

Saberi, S., Stauffer, J.E., Schulte, D.J., Ravits, J., 2015. Neuropathology of Amyotrophic Lateral Sclerosis and Its Variants. Neurol. Clin. https://doi.org/10.1016/j.ncl.2015.07.012

Saggioro, F.P., Neder, L., Stávale, J.N., Paixão-Becker, A.N.P., Malheiros, S.M.F., Soares, F.A., Pittella, J.E.H., Matias, C.C.M.S., Colli, B.O., Carlotti, C.G., Franco, M., 2014. Fas, FasL, and cleaved caspases 8 and 3 in glioblastomas: A tissue microarray-based study. Pathol. Res. Pract. 210, 267–273. https://doi.org/10.1016/j.prp.2013.12.012

Simpson, J.E., Fernando, M.S., Clark, L., Ince, P.G., Matthews, F., Forster, G., O'Brien, J.T., Barber, R., Kalaria, R.N., Brayne, C., Shaw, P.J., Lewis, C.E., Wharton, S.B., 2007. White matter lesions in an unselected cohort of the elderly: Astrocytic, microglial and oligodendrocyte precursor cell responses. Neuropathol. Appl. Neurobiol. 33, 410–419. https://doi.org/10.1111/j.1365-2990.2007.00828.x

Sjöbeck, M., Haglund, M., Persson, A., Sturesson, K., Englund, E., 2003. Brain tissue microarrays in dementia research: White matter microvascular pathology in Alzheimer's disease. Neuropathology 23, 290–295. https://doi.org/10.1046/j.1440-1789.2003.00515.x

Tang, Y., Le, W., 2016. Differential Roles of M1 and M2 Microglia in Neurodegenerative Diseases. Mol. Neurobiol. https://doi.org/10.1007/s12035-014-9070-5

Tully, P.J., Debette, S., Mazoyer, B., Tzourio, C., 2017. White Matter Lesions are Associated with Specific Depressive Symptom Trajectories among Incident Depression and Dementia Populations: Three-City Dijon MRI Study. Am. J. Geriatr. Psychiatry 25, 1311–1321. https://doi.org/10.1016/J.JAGP.2017.06.003

Veltema, A.N., 1975. The case of the saltimbanque prosper lecomte. A contribution to the study of the history of progressive muscular atrophy (aran-duchenne) and amyotrophic lateral sclerosis (charcot). Clin. Neurol. Neurosurg. 78, 204–209. https://doi.org/10.1016/S0303-8467(75)80050-3

Walker, L., McAleese, K.E., Johnson, M., Khundakar, A.A., Erskine, D., Thomas, A.J., McKeith, I.G., Attems, J., 2017. Quantitative neuropathology: an update on automated methodologies and implications for large scale cohorts. J. Neural Transm. 124, 671–683. https://doi.org/10.1007/s00702-017-1702-2

Waller, R., Baxter, L., Fillingham, D.J., Coelho, S., Pozo, J.M., Mozumder, M., Frangi, A.F., Ince, P.G., Simpson, J.E., Robin Highley, J., 2019. Iba-1-/CD68+ microglia are a prominent feature of age-associated deep subcortical white matter lesions. PLoS One

14. https://doi.org/10.1371/journal.pone.0210888

Wang, Huamin, Wang, Hua, Zhang, W., Fuller, G.N., 2006. Tissue Microarrays: Applications in Neuropathology Research, Diagnosis, and Education. Brain Pathol. 12, 95–107. https://doi.org/10.1111/j.1750-3639.2002.tb00426.x

Wen-Hui Wan, Fortuna, M.B., Furmanski, P., 1987. A rapid and efficient method for testing immunohistochemical reactivity of monoclonal antibodies against multiple tissue samples simultaneously. J. Immunol. Methods 103, 121–129. https://doi.org/10.1016/0022-1759(87)90249-3